RSC Advances

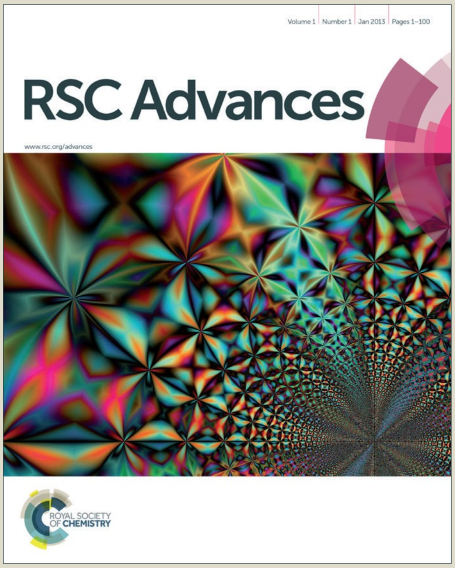

ROYAL SOCIETY OF CHEMISTRY

www.rsc.org/advances

Flower-like Bi_2S_3/Bi_2MoO_6 heterojunction superstructures with enhanced visible-light-driven photocatalytic activity

Junlei Zhang,[a] Lisha Zhang,*[a] Nuo Yu,[b] Kaibing Xu,[b] Shijie Li,[a] Huanli Wang,[a] and Jianshe Liu*[a]

[a] State Environmental Protection Engineering Center for Pollution Treatment and Control in Textile Industry, College of Environmental Science and Engineering, Donghua University, Shanghai 201620, China

[b] State Key Laboratory for Modification of Chemical Fibers and Polymer Materials, College of Materials Science and Engineering, Donghua University, Shanghai 201620, China

Abstract: A prerequisite for the development of photocatalytic technology is to obtain efficient visible-light-driven photocatalysts. Herein, we have reported flower-like Bi_2S_3/Bi_2MoO_6 heterojunction as a novel and efficient visible-light-driven photocatalyst. Bi_2S_3/Bi_2MoO_6 heterojunction has been prepared by a solvothermal method. It consists of flower-like superstructures with diameters ranging from 1 to 3 μm, which are built from Bi_2MoO_6 nanosheets with a thickness of about 15 nm decorated with Bi_2S_3 nanoparticles with diameter of ~3.5 nm. Furthermore, the photocatalytic activity of Bi_2S_3/Bi_2MoO_6 heterojunction has been evaluated through the degradation of rhodamine B (RhB) dye and colorless parachlorophenol (4-CP) under visible-light irradiation ($\lambda > 400$ nm). The results demonstrate that Bi_2S_3/Bi_2MoO_6 heterojunction exhibits higher photocatalytic activity in degrading RhB and 4-CP than single Bi_2S_3 or Bi_2MoO_6. More importantly, the photocatalytic

---

* Corresponding authors. Tel.: +86-21-67792548; Fax: +86-21-67792522.
E-mail address: lszhang@dhu.edu.cn (L.S. Zhang); liujianshe@dhu.edu.cn (J.S. Liu).

activity of Bi_2S_3/Bi_2MoO_6 heterojunction is superior to the sum of the activities of two individual photocatalysts (Bi_2MoO_6 and Bi_2S_3). The recycling experiment confirms that Bi_2S_3/Bi_2MoO_6 heterojunction is essentially stable during the photocatalytic process. Therefore, Bi_2S_3/Bi_2MoO_6 heterojunction can be used as an efficient and stable visible-light-driven photocatalyst for the purification of the environments.

Keywords: Bi_2S_3/Bi_2MoO_6; superstructures; visible-light-driven; photocatalysis

1. Introduction

Over the past few years, environmental problems, especially associated with harmful organic pollutants in water, are posing severe threats to human health. Among the widespread methods for the purification of the environments, semiconductor photocatalysis, as a “green” and energy saving technology for completely eliminating organic pollutants, has drawn worldwide attention.[1-4] A prerequisite for the development of photocatalytic technology is to obtain efficient photocatalysts.[1-4] Up to now, TiO_2 is undoubtedly one of the most excellent and widely used photocatalysts due to its abundance, chemical stability, low cost, and nontoxicity.[5, 6] But a major drawback of TiO_2 is its large bandgap (~3.2 eV), and thus only UV light (typically $\lambda < 400$ nm; a small fraction of the solar spectrum, ~5%) can be absorbed, which significantly limits the utilization of solar light in the visible region ($400 < \lambda < 700$ nm).[5, 6] To utilize solar energy more effectively, the development of efficient visible-light-driven (VLD) photocatalysts has drown worldwide attention.

Recently, bismuth(iii)-based semiconductor photocatalysts have been demonstrated to exhibit superior photocatalytic activities under visible-light irradiation ($\lambda > 400$ nm), since Bi

6s and O 2p levels can form a preferable hybridized conduction band (VB) to show strong oxidative ability for degrading organic pollutants.[7-19] Thus, a series of single-component bismuth(iii)-based photocatalysts have been developed, such as $CaBi_2O_4$,[7] Bi_2O_3,[8] $BiVO_4$,[9] Bi_2WO_6,[10, 11] BiOX (X=Cl, Br, I)[12] and Bi_2MoO_6[13-19]. Among these bismuth(iii)-based photocatalysts, bismuth molybdate (Bi_2MoO_6, band gap ~2.7 eV) possesses excellent photocatalytic performance for water splitting and organic pollutant degradation.[13-19] For instance, Kudo et al. have reported that Bi_2MoO_6 shows high photocatalytic activity for O_2 evolution under visible-light irradiation;[15] and several groups have confirmed that Bi_2MoO_6 exhibits excellent photocatalytic activity for the degradation of rhodamine B dye.[16-19] However, there are still some drawbacks hindering their practical application, such as the unsatisfactory photo-response range and short photogenerated electron-hole pair lifetime.[13-19]

It is well known that the construction of semiconductor heterojunctions is an efficient method for the improvement of photocatalytic performances, as summarized in our recent review.[3] To improve the photocatalytic activity of Bi_2MoO_6, several kinds of Bi_2MoO_6-based heterojunctions have been developed, including Bi_2MoO_6-oxide (oxide: TiO_2,[20] ζ-Bi_2O_3,[21] CuPc,[22] BiOCl,[23] $ZnTiO_3$,[24] and $Bi_2O_2CO_3$[25]), Bi_2MoO_6-metal (metal: Ag[26] and W[27]), Bi_2MoO_6-carbon (carbon: graphene[28] and carbon nanofibers[29]), multicomponent (such as Ag-AgBr-Bi_2MoO_6[30] and Ag-AgCl-Bi_2MoO_6[31]). Compared with pure Bi_2MoO_6, these Bi_2MoO_6-based heterojunctions exhibit higher photocatalytic activity for the degradation of organic pollutants, hydrogen generation, and/or photocatalytic disinfection.[20-32] However, to the best of our knowledge, there is little work that reports on the development of Bi_2MoO_6-sulfide heterojunction photocatalysts, except for MoS_2/Bi_2MoO_6.[32]

As a lamellar binary semiconductor, bismuth sulfide (Bi_2S_3) has significant applications in photovoltaics and photocatalysis. Several kinds of Bi_2S_3 heterojunctions have been demonstrated to exhibit excellent photocatalytic activity, such as Bi_2S_3/Bi_2WO_6[33] and Bi_2S_3/BiOX (X=Cl, Br, I)[34-36]. Moreover, the size quantization enables Bi_2S_3 nanoparticles (1.3 eV for bulk) to show tunable photosensitization and considerable photoactivity in the visible region.[37] Herein, to improve the photocatalytic activity of Bi_2MoO_6, we designed and constructed Bi_2S_3/Bi_2MoO_6 heterojunction as a novel photocatalyst. Bi_2S_3/Bi_2MoO_6 heterojunction was prepared via a solvothermal method, and it consisted of flower-like superstructures with diameters ranging from 1 to 3 μm, which were built from Bi_2MoO_6 nanosheets decorated with Bi_2S_3 nanoparticles (~3.5 nm). Importantly, under visible-light irradiation, Bi_2S_3/Bi_2MoO_6 heterojunction exhibited higher photocatalytic activity in degrading rhodamine B (RhB) dye and colorless parachlorophenol (4-CP) than single Bi_2S_3 or Bi_2MoO_6.

2. Experimental Details

2.1 Materials

Bismuth nitrate pentahydrate ($Bi(NO_3)_3{\cdot}5H_2O$), sodium molybdate ($Na_2MoO_4{\cdot}2H_2O$), thiourea ($(NH_2)_2CS$), absolute ethanol (CH_3CH_2OH) and ethylene glycol were purchased from Sinopharm Chemical Reagent Co., Ltd (P.R. China). Rhodamine B (RhB) was purchased from Sigma (America) and parachlorophenol (4-CP) was purchased from J&K CHEMICAL Ltd. (P.R. China). All chemicals were of analytical grade and were used as received without further purification.

2.2. Preparation of photocatalysts

Bi_2S_3/Bi_2MoO_6 heterojunction was prepared via a solvothermal method. In a typical procedure, $Bi(NO_3)_3\cdot 5H_2O$ (2.1 mmol) and $Na_2MoO_4\cdot 2H_2O$ (1 mmol) were ultrasonically dissolved in 10 mL ethylene glycol, respectively. Meanwhile, $(NH_2)_2CS$ (0.15 mmol) was ultrasonically dissolved in 60 mL absolute ethanol. Subsequently, Na_2MoO_4 solution and $(NH_2)_2CS$ solution were added in turn to $Bi(NO_3)_3$ solution. The resulting precursor solution was agitated for about 10 min, then transferred to a 100 mL autoclave, sealed, and solvothermally treated at 160 °C for 12 h. The system was cooled to room temperature naturally, and the solid sample was collected by filtration, washed thoroughly with water and ethanol and dried at 60 °C for 24 h. For comparison, pure Bi_2MoO_6 and Bi_2S_3 sample were also respectively prepared by adopting the same method in the absence of $(NH_2)_2CS$ or Na_2MoO_4 $2H_2O$.

2.3. Characterization of photocatalysts

X-ray diffraction (XRD) measurements were recorded on a D/max-2550 PC X-ray diffractometer using Cu Ka radiation (λ = 0.15418 nm). The scanning electron microscope (SEM) characterizations were performed on a Hitachi S-4800 field emission scanning electron microscope. The transmission electron microscope (TEM) analyses were performed by a JEOL JEM-2100 high-resolution transmission electron microscope. The optical diffuse reflectance spectrum were conducted on a UV-VIS-NIR scanning spectrophotometer (Lambda 35, PerkinElmer) using an integrating sphere accessory. The electronic states of elements in the sample were analyzed by using X-ray photoelectron spectroscopy (PHI-5400, PerkinElmer). The Brunauer-Emmett-Teller (BET) surface area was determined by a multipoint BET method using the adsorption data in the relative pressure (P/P_0) range of

0.05-0.3. A desorption isotherm was used to determine the pore size distribution via the Barret-Joyner-Halender (BJH) method, assuming a cylindrical pore model.

2.4. Photocatalytic activity

Photocatalytic activities of as-prepared photocatalysts were evaluated by degrading the aqueous solution of rhodamine B (RhB) dye or colorless parachlorophenol (4-CP) under visible-light irradiation using a 300 W xenon lamp (Beijing Perfect Light Co. Ltd., Beijing) with a cut-off filter ($\lambda > 400$ nm) as light source. In each experiment, 30 mg of photocatalyst was added to 50 mL of RhB (10 mg L^{-1}, pH = 6.27) or 4-CP (1 mg L^{-1}, pH = 6.34) solution. Prior to irradiation, the suspension was mildly magnetically stirred in the dark for 30 min to ensure that an adsorption/desorption equilibrium was established between the photocatalysts and the target contaminant (RhB or 4-CP). During visible-light irradiation, 2 mL suspension was collected at given time intervals and then centrifuged to remove the remaining solids for analysis. For the photocatalytic test of RhB, the UV-vis absorption spectra of the solutions were recorded on a U-2910 UV-vis spectrophotometer (Hitachi, Japan), and then RhB concentration was calculated by analyzing the photoabsorption intensity at wavelength of 554 nm. For the photocatalytic test of 4-CP, the 4-CP concentrations in the solutions were analyzed by high-performance liquid chromatography (HPLC) using an Dionex Ultimate 3000 series (USA) equipped with a diode array detector (DAD) with wavelength set at 280 nm directly after filtration through a 0.22 μm hydrofacies syringe filter. The mobile phase was methanol (80%) and water (20%) and the flow rate was 0.5 mL min^{-1}. In the stability and reusability test of the catalyst, four consecutive cycles were tested. The catalysts were washed thoroughly with water and dried after each cycle, and then it was immersed in the same volume (50 mL) of fresh parachlorophenol aqueous solution (1 mg L^{-1}) again.

Total organic carbon (TOC) analysis was carried out by adding 300 mg Bi_2S_3/Bi_2MoO_6 into 100 mL RhB aqueous solution (60 mg L^{-1}). Prior to irradiation, the suspension was magnetically stirred for 60 min in the dark to achieve a saturated RhB absorption onto the photocatalyst surface. During visible-light irradiation, 10 mL suspension was collected at given time intervals and filtered by the membrane pore size of 0.45 μm to remove the photocatalyst, and then was detected by a Shimadzu TOC-VCPH total organic carbon analyzer.

3. Results and discussion

3.1 Preparation and characterization of catalysts

Bi_2S_3/Bi_2MoO_6 heterojunction was prepared by a one-step solvothermal method. Bi_2MoO_6 was produced by the reaction of $Bi(NO_3)_3$ (2 mmol) and Na_2MoO_4 (1 mmol) and then crystallized during the solvothermal process. The redundant $Bi(NO_3)_3$ (0.1 mmol) molecules were adsorbed on the surface of Bi_2MoO_6. Sulfur ions were slowly released from $(NH_2)_2CS$ in the solvothermal process, resulting in the in situ growth of Bi_2S_3 nanoparticles on Bi_2MoO_6 superstructures to form Bi_2S_3/Bi_2MoO_6 heterojunction (theoretical molar ratio of Bi_2S_3:Bi_2MoO_6 was 1:20).

The phase of the as-prepared Bi_2S_3/Bi_2MoO_6 heterojunction was investigated by XRD pattern (Fig. 1). For comparison, the XRD patterns of pure Bi_2MoO_6 and Bi_2S_3 were also recorded. All diffraction peaks from pure Bi_2MoO_6 can be readily indexed to orthorhombic Bi_2MoO_6 (JCPDS No. 21-0102), and the diffraction peaks for pure Bi_2S_3 can be assigned to orthorhombic Bi_2S_3 (JCPDS No. 17-0320). Bi_2S_3/Bi_2MoO_6 sample exhibits a XRD pattern which is similar to that of pure Bi_2MoO_6; four strong diffraction peaks at 28.3°, 32.6°, 46.7°

and 55.6° can be assigned to (131), (002), (202) and (133) planes of orthorhombic Bi_2MoO_6. In addition, no characteristic peaks peculiar to Bi_2S_3 are observed, which may be attributed to the fact that the content of Bi_2S_3 in Bi_2S_3/Bi_2MoO_6 was too low to be efficiently detected.

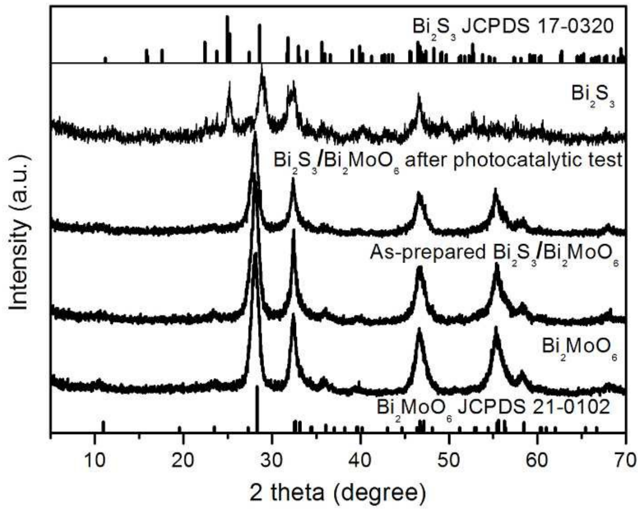

Fig. 1. XRD patterns of Bi_2MoO_6, Bi_2S_3, as-prepared Bi_2S_3/Bi_2MoO_6 and the used Bi_2S_3/Bi_2MoO_6 after photocatalytic test, and standard XRD patterns of Bi_2MoO_6 (JCPDS 21-0102) and Bi_2S_3 (JCPDS 17-0320).

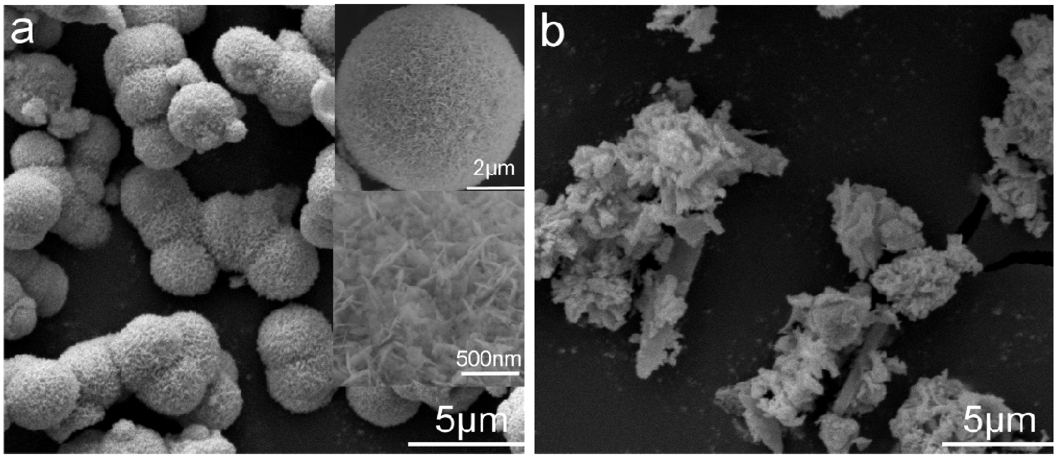

Fig. 2. SEM images of pure Bi_2MoO_6 (a) and pure Bi_2S_3 (b).

Subsequently, the sizes and morphologies of Bi_2S_3/Bi_2MoO_6 heterojunction as well as pure Bi_2MoO_6 and Bi_2S_3 were further studied by SEM and TEM images (Fig. 2, 3). Obviously, pure Bi_2MoO_6 sample consists of flower-like microspheres with diameters ranging from 1 to 3 μm (Fig. 2a). The close-up view indicates that Bi_2MoO_6 flower-like superstructure is in fact built from nanosheets (inset of Fig. 2a). Meanwhile, pure Bi_2S_3 sample presents the irregular large-size flake structure (Fig. 2b). In addition, Bi_2S_3/Bi_2MoO_6 sample is also composed of flower-like superstructures with diameters ranging from 1 to 3 μm (Fig. 3a), which is similar to that of pure Bi_2MoO_6 sample. These superstructures are in fact built from two dimensional nanosheets with a thickness of about 15 nm and an average length of about 200 nm (Fig. 3b), which can be vividly demonstrated by the part view (Fig. 3c) at higher magnification. More importantly, more hierarchical nanopores and macro-pores superstructures with bigger diameter sizes in nanosheets are obtained by Bi_2S_3/Bi_2MoO_6 heterojunction compared with pure Bi_2S_3 and pure Bi_2MoO_6, and these hierarchical porous superstructures may improve the physicochemical properties or serve as transport paths for small molecules, are found among the nanosheets in the spherical superstructures (Fig. 3c).

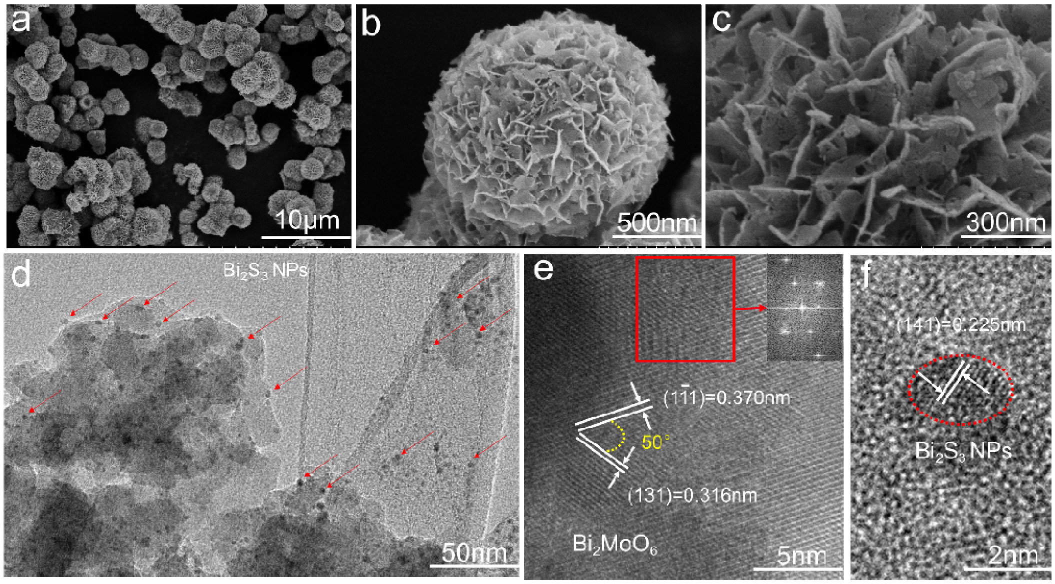

Fig. 3. SEM (a-c) and TEM (d-f) images of Bi_2S_3/Bi_2MoO_6 heterojunction.

Further information about Bi_2S_3/Bi_2MoO_6 heterojunction is obtained from TEM image (Fig. 3d), and it confirms that the flower-like superstructure is built from nanosheets. The lattice resolved high-resolution TEM image (Fig. 3e) and its corresponding Fourier transform

(FFT) pattern (inset of Fig. 3e) clearly exhibit the (131) and $(1\bar{1}1)$ crystal planes with 0.316 nm and 0.370 nm *d*-spacings and 50° interfacial angle, further indicating the orthorhombic structure of Bi_2MoO_6. Importantly, one can find that there are plenty of small nanoparticles with the size of ~3.5 nm anchored on the surface of nanosheets (Fig. 3d), and these small nanoparticles exhibit lattice fringes with an interplane spacing of 0.225 nm, which is corresponding to the (141) crystal plane of orthorhombic Bi_2S_3 (Fig. 3f). In addition, the EDS (Fig. 4) confirms the presence of Bi, Mo, O and S elements in the Bi_2S_3/Bi_2MoO_6 sample.

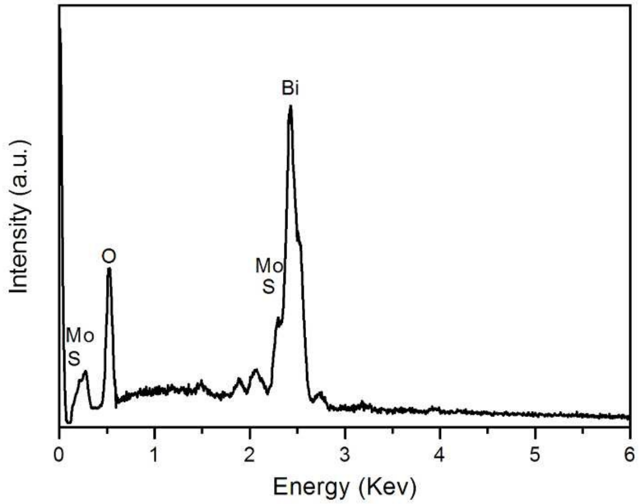

Fig. 4 EDS pattern of Bi_2S_3/Bi_2MoO_6 heterojunction.

Furthermore, the elemental composition and chemical status of Bi_2S_3/Bi_2MoO_6 sample was investigated by X-ray photoelectron spectroscopy (XPS). The survey spectrum in Fig. 5a clearly demonstrates that the sample is mainly composed of Bi, Mo, O and S elements. The binding energies (Fig. 5b) of 158.3 eV for Bi $4f_{7/2}$ and 163.6 eV for Bi $4f_{5/2}$ indicate a trivalent oxidation state for bismuth.[32] Fig. 5c shows that the binding energies of Mo $3d_{3/2}$ and Mo $3d_{5/2}$ peaks in sample are respectively located at 234.5 and 231.4 eV, suggesting that Mo^{6+} exists in the Bi_2S_3/Bi_2MoO_6 sample.[32] Meanwhile, Fig. 5d gives the binding energies of S

$2p_{1/2}$ and S $2p_{3/2}$ peaks in sample, which are respectively located in 158.3 and 163.6 eV, indicating that S^{2-} exists in Bi_2S_3/Bi_2MoO_6 sample.[34] These results support the formation of Bi_2S_3 and Bi_2MoO_6 in the sample.

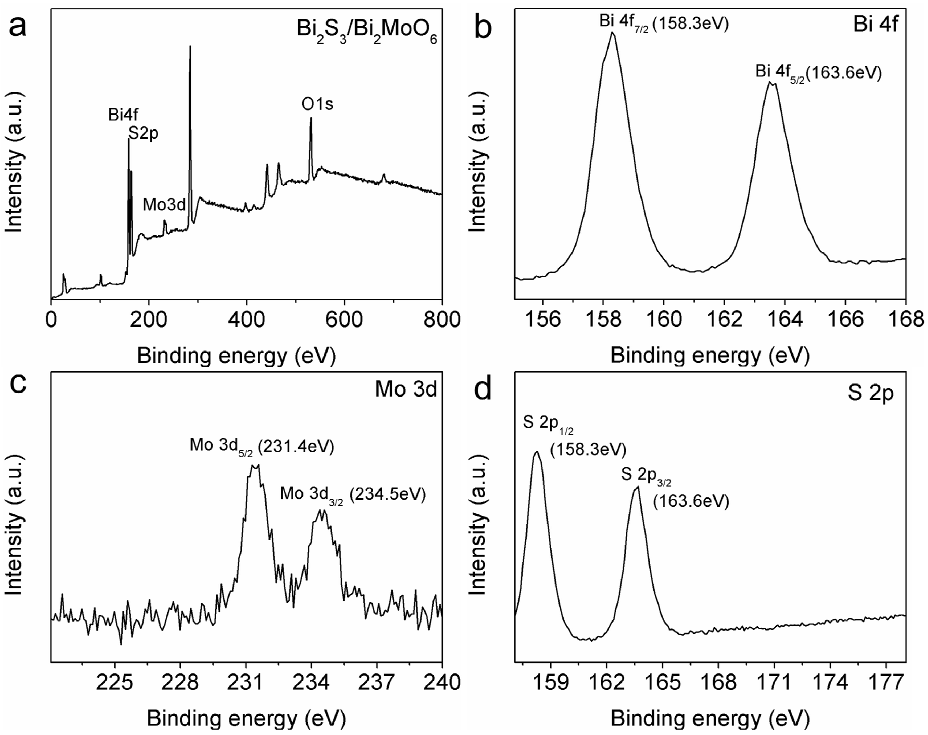

Fig. 5 (a) Survey XPS spectrum of Bi_2S_3/Bi_2MoO_6 heterojunction. High-resolution XPS spectra of Bi 4f (b), Mo 3d (c) and S 2p (d) from Bi_2S_3/Bi_2MoO_6 heterojunction.

Based on the above XRD, TEM, EDS and XPS results, one can conclude that there are Bi_2S_3 and Bi_2MoO_6 species in the Bi_2S_3/Bi_2MoO_6 sample, and the nanojunction in Bi_2S_3/Bi_2MoO_6 system is well constructed. Subsequently, the nitrogen adsorption/desorption isotherms of Bi_2MoO_6 and Bi_2S_3/Bi_2MoO_6 heterojunction were investigated (Fig. 6a). The Brunauer-Emmett-Teller (BET) surface area of Bi_2MoO_6 is calculated to be 65.7 m^2 g^{-1}. Interestingly, Bi_2S_3/Bi_2MoO_6 heterojunction exhibits a slight increase of BET surface area (74.9 m^2 g^{-1}). Usually, an increase of the surface area leads to an improvement of the photocatalytic activity. Moreover, the pore size distributions, which are calculated from the desorption branches, reveal the existence of nano-pores in both Bi_2MoO_6 and Bi_2S_3/Bi_2MoO_6

heterojunction (the inset of Fig. 6a). The nanopores in Bi_2MoO_6 have the diameter of about 15.4 nm, while those in Bi_2S_3/Bi_2MoO_6 heterojunction have the diameter of about 14.4 nm, which agrees with that revealed by the SEM and TEM images (Fig. 2a and Fig. 3a-c). The presence of nanopores may greatly improve the physicochemical properties and/or serve as transport paths for small molecules.

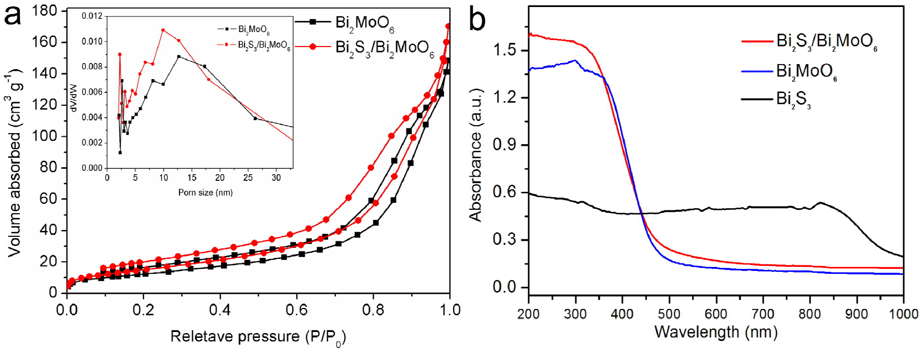

Fig. 6 (a) Nitrogen adsorption–desorption isotherms of pure Bi_2MoO_6 and Bi_2S_3/Bi_2MoO_6 heterojunction; (b) Uv-vis diffuse reflectance spectra of pure Bi_2MoO_6, bulk Bi_2S_3 and Bi_2S_3/Bi_2MoO_6 heterojunction.

The optical absorption of Bi_2S_3/Bi_2MoO_6 heterojunction was measured by an UV-vis spectrometer (Fig. 6b). For comparison, the optical absorption spectra of pure Bi_2MoO_6 and bulk Bi_2S_3 were also recorded. Pure Bi_2MoO_6 exhibits strong photoabsorption from the UV to visible-light region with an absorption edge around 470 nm (band gap: 2.7 eV). In addition, bulk Bi_2S_3 shows intense absorption over the visible-light range, even extending to the infrared region. The fitted direct band gap of Bi_2S_3 is determined to be 1.30 eV, which is equal to its bulk value. Interestingly, Bi_2S_3/Bi_2MoO_6 heterojunction displays strong photoabsorption from the UV to visible-light region with an absorption edge around 480 nm, which is similar to that of pure Bi_2MoO_6. Obviously, the presence of Bi_2S_3 nanoparticles (NPs) in Bi_2S_3/Bi_2MoO_6 heterojunction has no obvious effect on its optical absorption, which should result from the small size and is similar to the previous study.[37] On the basis of the effective mass approximation model, the blue shift of Bi_2S_3 NPs relative to the bulk is dominated by the confinement of electrons and holes, as described by the following equation:[37, 38]

$$\Delta E_g(R) = \frac{h^2}{8m_0R^2}\left(\frac{1}{m_e^*} + \frac{1}{m_h^*}\right)$$

where $\Delta E_g(R)$ is the band gap shift for the crystal radius *R*, *h* is the Planck's constant, m_0 is the electron mass, while m_e^* and m_h^* are the effective masses of electrons and holes, respectively. Since Bi_2S_3 NPs exhibit the average diameter of ~3.5 nm (Fig. 3d. f), the calculated band gap should be 2.9 eV which is close to that of (2.7 eV) Bi_2MoO_6.

The band edge positions of Bi_2MoO_6 (2.64 eV), bulk Bi_2S_3 (1.3 eV) and Bi_2S_3 NPs (2.9 eV) can be evaluated by the following empirical equation:[39] $E_{VB} = X - E_0 + 0.5E_g$ (1); $E_{CB} = E_{VB} - E_g$ (2), where E_{VB} is the valence band (VB) edge potential, X is the electronegativity of the semiconductor, which is the geometric mean of the electronegativity of the constituent atoms. The X values for Bi_2MoO_6 and Bi_2S_3 are calculated as 5.50 eV[40] and 5.95 eV[33], respectively. E_0 is the energy of free electrons on the hydrogen scale (about 4.5 eV), and E_g is the band gap energy of the semiconductor. According to the Eqs. (1) and (2), E_{VB} and E_{CB} values of Bi_2MoO_6 are determined to be 2.32 eV and -0.32 eV, those of bulk Bi_2S_3 are 2.1 eV and 0.8 eV, and those of Bi_2S_3 NPs (~3.5 nm) are 2.90 eV and 0 eV. The VB of Bi_2S_3 shifts to more positive potentials to produce the larger VB energy difference (ΔE_V) between Bi_2MoO_6 and Bi_2S_3, which further favors the electrons transfer and strong oxidization ability of holes.

3.2 Photocatalytic performances under visible-light irradiation

Rhodamine B (RhB), a common dye widely used in dyeing cellulose, nylon, silk and wool, was firstly chosen as a representative pollutant to evaluate the photocatalytic performance of Bi_2S_3/Bi_2MoO_6 heterojunction (Fig. 7). For comparison, RhB degradation without photocatalyst (blank test) and with pure Bi_2MoO_6 or pure Bi_2S_3, was also performed under the other identical conditions, respectively. When dissolved in distilled water, RhB displays a major absorption band centered at 554 nm that is used to monitor the photocatalytic degradation. Clearly, Bi_2MoO_6, Bi_2S_3 and Bi_2S_3/Bi_2MoO_6 heterojunction can reach the absorption equilibrium within 30 min in the dark and Bi_2S_3/Bi_2MoO_6 heterojunction can adsorb RhB molecules more efficiently (44.3%) than pure Bi_2MoO_6 (0.021%) and pure Bi_2S_3 (0.005%) due to the larger surface area.

Subsequently, the photocatalytic reaction was carried out for another 60 min under visible-light irradiation (Fig. 7). The blank test indicates that the degradation of RhB is extremely slow without photocatalyst under visible-light irradiation. By using the bulk Bi_2S_3 as the VLD photocatalyst, the degradation of RhB is also slow, and only 14% RhB can be removed after 60 min of reaction. When pure Bi_2MoO_6 is used as the VLD photocatalyst, the photodegradation efficiency of RhB can just approach 29% after 60 min, indicating low photocatalytic activity. Importantly, when Bi_2S_3/Bi_2MoO_6 heterojunction is used as the VLD photocatalyst, 100% RhB can be removed after 60 min of visible-light irradiation, indicating the highest photocatalytic activity. Furthermore, the photocatalytic degradation rate was calculated by the apparent pseudo-first-order model (the inset of Fig. 7). The rate from Bi_2S_3/Bi_2MoO_6 heterojunction was determined to be 0.0643 min^{-1} which is greatly higher than that from the pure Bi_2S_3 (0.000195 min^{-1}) and pure Bi_2MoO_6 (0.000493 min^{-1}). These facts indicate that the construction of Bi_2S_3/Bi_2MoO_6 heterojunction improve greatly the photocatalytic performances, which is similar to the previous reports on heterojunction photocatalysts such as Alpha-beta-Ga_2O_3 junction[41,42], $Sr_2TiO_4/SrTiO_3$ (La,Cr) heterojunction[43] and $Ga_2O_3/ZnGa_2O_4$ heterojunction[44].

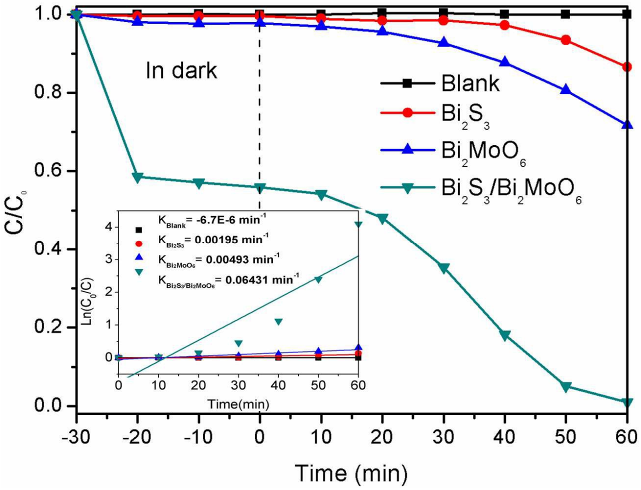

Fig. 7 The adsorption and degradation efficiency of RhB in aqueous solution (10 mg L^{-1}, 50 mL, pH = 6.27) versus the exposure time under visible-light irradiation (λ > 400 nm), in the absence of photocatalyst and in the presence of as-prepared samples (30 mg).

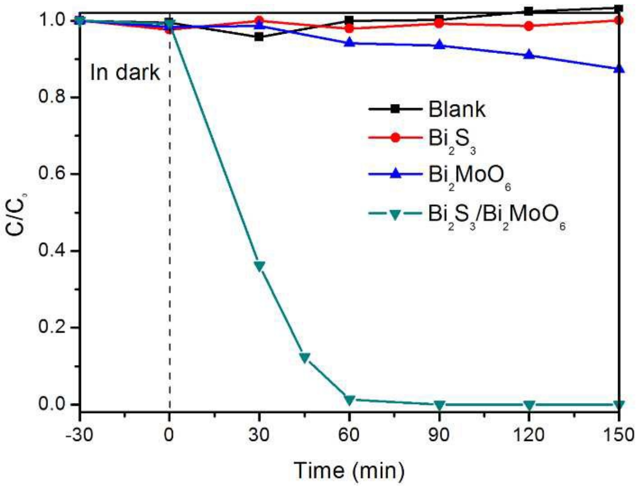

Fig. 8 The adsorption and degradation efficiency of 4-CP in aqueous solution (1 mg L^{-1}, 50 mL, pH = 6.34), versus the exposure time under visible-light irradiation (λ > 400 nm), in the absence of photocatalyst and in the presence of as-prepared samples (30 mg).

To further illustrate the fact that the real photocatalytic performance of Bi_2S_3/Bi_2MoO_6 heterojunction results from the excitation of the photocatalyst rather than the sensitization mechanism, colorless parachlorophenol (4-CP) was used as the model of pollutants (Fig. 8). Obviously, no 4-CP can be absorbed by all these photocatalysts for 30 min of dark reaction, which should be attributed to the nature of the electrically neutral of 4-CP. In the subsequent photocatalytic reaction process, the degradation of 4-CP without photocatalyst and with bulk Bi_2S_3, is extremely slow and nearly no 4-CP is removed after 150 min of visible-light irradiation. By using pure Bi_2MoO_6 as the VLD photocatalyst, 4-CP degradation is also very slow and only 13% 4-CP is photocatalytically degraded after 150 min of visible-light irradiation. Surprisingly, when Bi_2S_3/Bi_2MoO_6 heterojunction is used as the VLD photocatalyst, 4-CP in the solution is rapidly photocatalytically decomposed during 60 min of visible-light irradiation, and the photodegradation efficiency reaches up to 98.7% at 60 min. When the illumination time lasts to 90 min, 100% 4-CP has been removed, indicating the highest photocatalytic activity of Bi_2S_3/Bi_2MoO_6 heterojunction among these above-mentioned photocatalysts.

In order to further confirm the role of the nanojunction in Bi_2S_3/Bi_2MoO_6 heterojunction, the removal efficiencies of RhB and 4-CP were compared (Fig. 9). When pure Bi_2MoO_6 is used as the VLD photocatalyst, 29% RhB is removed after 60 min, and the removal efficiency of 4-CP can reach 13% after 150 min. By using pure Bi_2S_3 as the VLD photocatalyst, only 14% RhB is removed after 60 min, and nearly no 4-CP is degraded after 150 min. Thus, the total degradation efficiencies by two individual photocatalysts (Bi_2MoO_6 and Bi_2S_3) are 42% (29% + 13%) for RhB after 60 min, or 14% (14% + 0) for 4-CP after 150 min. More importantly, Bi_2S_3/Bi_2MoO_6 heterojunction can remove 100% RhB after 60 min or 100% 4-CP after 90 min, which are both higher than the total removal efficiencies (42% and 14%) by pure Bi_2MoO_6 and Bi_2S_3 for RhB and 4-CP removal. These results strongly reveal that there is a synergic effect in Bi_2S_3/Bi_2MoO_6 heterojunction, which is similar to the phenomenon in our previous study.[45,46]

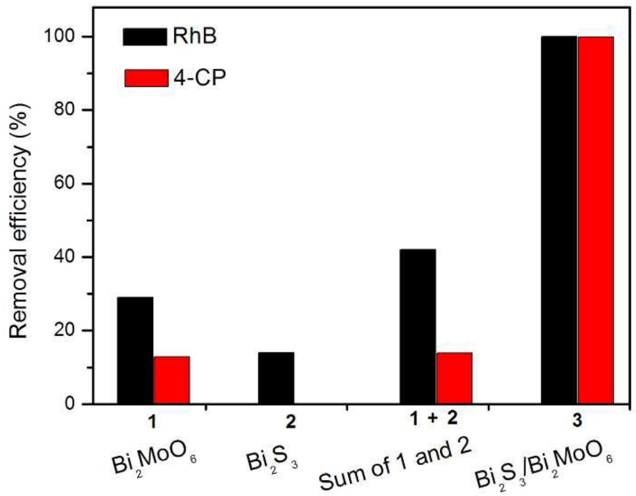

Fig. 9 The comparison of removal efficiencies of RhB after 60 min and 4-CP after 150 min, by Bi_2MoO_6, Bi_2S_3 and Bi_2S_3/Bi_2MoO_6 heterojunction.

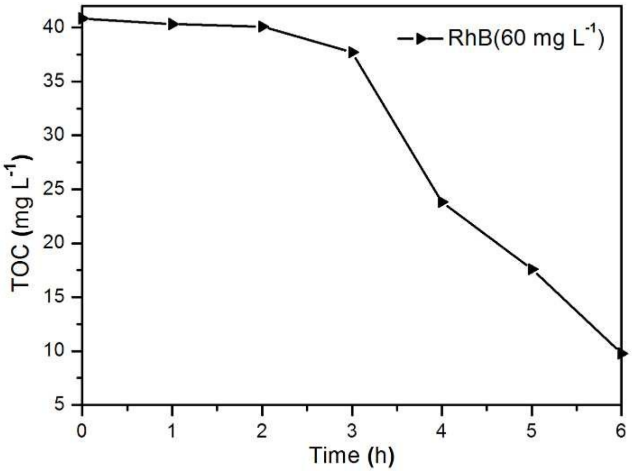

Fig. 10 TOC removal during RhB (60 mg L^{-1}, 100 mL) photocatalytic degradation process by Bi_2S_3/Bi_2MoO_6 heterojunction (300 mg).

It is well known that the mineralization is the ultimate goal in pollutant treatment, and total organic carbon (TOC) value is usually used as an important index for the mineralization degree of organic species. Herein, the mineralization of RhB was investigated by immersing 300 mg Bi_2S_3/Bi_2MoO_6 in 100 mL RhB aqoeous solution (60 mg L^{-1}) under visible-light irradiation, and TOC value was recorded during the photocatalytic process (Fig. 10). Obviously, with the increase of irradiation time, the TOC concentration continuously decreases, indicating that RhB is steadily mineralized. After six hours, the TOC concentration decreases from 40.85 mg L^{-1} at 0 h to 9.791 mg L^{-1} at 6 h, reaching a high mineralization ratio of 76%. This fact demonstrates that Bi_2S_3/Bi_2MoO_6 heterojunction superstructures can efficiently degrade and mineralize organic pollutants under visible-light irradiation.

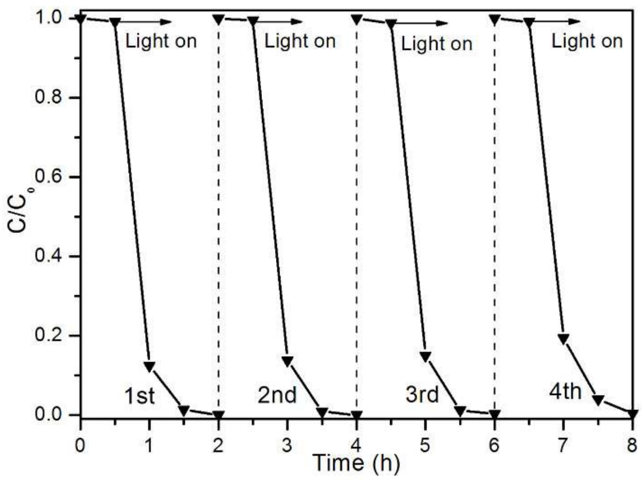

Fig. 11. Cycling runs in photocatalytic degradation of 4-CP over Bi_2S_3/Bi_2MoO_6 heterojunction.

The stability of Bi_2S_3/Bi_2MoO_6 heterojunction was also studied through the degradation of 4-CP under visible-light irradiation (Fig. 11). It should be noted that the Bi_2S_3/Bi_2MoO_6 heterojunction is easily recycled by simple filtration without any treatment in these experiments. After four cycles of the photodegradation process of 4-CP, the Bi_2S_3/Bi_2MoO_6 heterojunction does not exhibit any significant loss of activity, as shown in Fig. 11, confirming that the components of the Bi_2S_3/Bi_2MoO_6 heterojunction is not corroded by light and that the heterojunction structure is stable during the photocatalytic process. This fact can be further supported by XRD patterns, which reveal that Bi_2S_3/Bi_2MoO_6 heterojunction after the photocatalytic reaction exhibits the similar diffraction peaks compared with that of the as-prepared Bi_2S_3/Bi_2MoO_6 heterojunction (Fig. 1). Therefore, the as-prepared Bi_2S_3/Bi_2MoO_6 heterojunction is an effective and stable VLD photocatalyst.

Based on the above results, one can conclude that Bi_2S_3/Bi_2MoO_6 heterojunction exhibits higher photocatalytic activity than the pure Bi_2MoO_6 and pure Bi_2S_3 (Fig. 7, 8), and even higher than the sum of two individual photocatalysts (Bi_2MoO_6 and Bi_2S_3) for the photocatalytic degradation of RhB or 4-CP (Fig. 9). The possible reasons for the higher photocatalytic activity of Bi_2S_3/Bi_2MoO_6 heterojunction are analyzed, and we believe that there are chiefly two reasons. One reason is the hierarchical nanopores of Bi_2S_3/Bi_2MoO_6 heterojunction compared with Bi_2MoO_6 and Bi_2S_3 as shown in Fig. 3a-c and Fig. 2a, b. Undoubtedly, these hierarchical porous superstructures can improve the physicochemical properties and be served as transport paths for small molecules, further facilitating the absorption and photodegradation of RhB and 4-CP. The other reason should be due to the efficient separation of photogenerated electron-hole pairs.[41-44] Obviously, more matching band gaps are thus obtained due to the presence of Bi_2S_3 nanoparticles (NPs) in Bi_2S_3/Bi_2MoO_6 heterojunction, further facilitating the separation of photogenerated electrons and holes. The energy band diagram and photocatalytic process of Bi_2S_3/Bi_2MoO_6 heterojunction can be proposed, as shown in Fig. 12. Under visible-light irradiation, the photocatalytic reaction is initiated by the absorption of visible-light photons with energy equal or higher than the band-gap in either Bi_2S_3 or Bi_2MoO_6 semiconductors, which results in the creation of photogenerated holes in its VB and electrons in its conduction band (CB). Since the CB and VB of Bi_2MoO_6 lie above those of Bi_2S_3 NPs, the photogenerated electrons easily migrate from the CB of Bi_2MoO_6 to that of Bi_2S_3 NPs; and the photogenerated holes can also be easily transferred from the VB of Bi_2S_3 NPs to that of Bi_2MoO_6. As a result, less of a barrier exists due to the promoted separation and migration of photogenerated carriers by the internal field. So the probability of electron-hole recombination can be decreased. Larger numbers of electrons stored on the Bi_2S_3 NPs surface and holes stored on the Bi_2MoO_6 surface can, respectively, participate in photoredox reactions to degrade organic pollution directly or indirectly, which can enhance the photocatalytic reaction greatly.

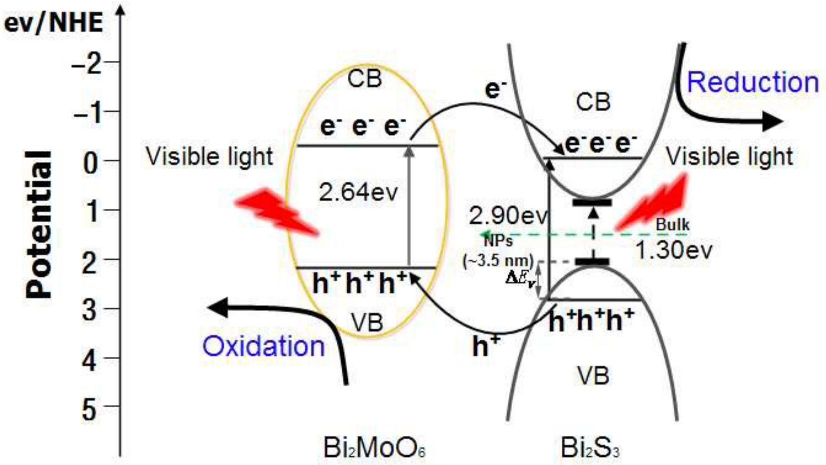

Fig. 12 The proposed possible mechanism for the improvement of photocatalytic activity.

4. Conclusions

In summary, Bi_2S_3/Bi_2MoO_6 heterojunction has been prepared by a simple solvothermal synthesis method. It consists of flower-like superstructures with diameters ranging from 1 to 3 μm, which are built from Bi_2MoO_6 nanosheets with a thickness of about 15 nm decorated with Bi_2S_3 nanoparticles with diameter of ~3.5 nm. The Bi_2S_3/Bi_2MoO_6 heterojunction displays higher efficient visible-light-driven photocatalytic activity in degradation of RhB and 4-CP, even higher than the sum of the activities of two individual photocatalysts (Bi_2MoO_6 and Bi_2S_3). Moreover, Bi_2S_3/Bi_2MoO_6 heterojunction can efficiently mineralize organic pollutants and be re-used due to excellent stability. Therefore, Bi_2S_3/Bi_2MoO_6 heterojunction has great potential as an efficient and stable visible-light-driven photocatalyst for water environmental purification and remediation application.

Acknowledgements

This work was financially supported by the National Natural Science Foundation of China (Grant Nos. 21377023 and 21477019), the Fundamental Research Funds for the Central Universities, and DHU Distinguished Young Professor Program.

References

1 M. R. Hoffmann, S. T. Martin, W. Y. Choi and D. W. Bahnemann, *Chem. Rev.*, 1995, 95, 69-96.

2 A. Kubacka, M. Fernandez-Garcia and G. Colon, *Chem. Rev.*, 2012, 112, 1555-1614.

3 H. Wang, L. Zhang, Z. Chen, J. Hu, S. Li, Z. Wang, J. Liu and X. Wang, *Chem. Soc. Rev.*, 2014, 43, 5234-5244.

4 J. Liu, Y. Liu, N. Liu, Y. Han, X. Zhang, H. Huang, Y. Lifshitz, S. T. Lee, J. Zhong and Z. Kang, *Science*, 2015, 347, 970-974.

5 X. Chen and S. S. Mao, *Chem. Rev.*, 2007, 107, 2891-2959.

6 X. Chen, L. Liu, P. Y. Yu and S. S. Mao, *Science*, 2011, 331, 746-750.

7 J. W. Tang, Z. G. Zou and J. H. Ye, *Angew. Chem. Int. Ed.*, 2004, 43, 4463-4466.

8 L. S. Zhang, W. Z. Wang, J. Yang, Z. G. Chen, W. Q. Zhang, L. Zhou and S. W. Liu., *Appl. Catal. A-Gen.*, 2006, 308, 105-110.

9 R. Li, F. Zhang, D. Wang, J. Yang, M. Li, J. Zhu, X. Zhou, H. Han and C. Li, *Nat. Commun.*, 2013, 4, 1432.

10 L. S. Zhang, W. Z. Wang, L. Zhou and H. Xu, *Small*, 2007, 3, 1618-1625.

11 L. S. Zhang, H. L. Wang, Z. G. Chen, P. K. Wong and J. S. Liu, *Appl. Catal. B-Environ.*, 2011, 106, 1-13.

12 H. Cheng, B. Huang, and Y. Dai, *Nanoscale*, 2014, 6, 2009-2026.

13 L. Zhang, T. Xu, X. Zhao and Y. Zhu, *Appl. Catal. B-Environ.*, 2010, 98, 138-146.

14 W. Yin, W. Wang and S. Sun, *Catal. Commun.*, 2010, 11, 647-650.

15 Y. Shimodaira, H. Kato, H. Kobayashi and A. Kudo, *J. Phys. Chem. B*, 2006, 110, 17790-17797.

16 Y. Ma, Y. Jia, Z. Jiao, M. Yang, Y. Qi and Y. Bi, *Chem. Commun.*, 2015, 51, 6655-6658.

17 J. Long, S. Wang, H. Chang, B. Zhao, B. Liu, Y. Zhou, W. Wei, X. Wang, L. Huang and W. Huang, *Small*, 2014, 10, 2791-2795.

18 Z. Li, X. Chen and Z. Xue, *Crystengcomm*, 2013, 15, 498-508.

19 M. Zhang, C. Shao, P. Zhang, C. Su, X. Zhang, P. Liang, Y. Sun and Y. Liu, *J. Hazard. Mater.*, 2012, 225, 155-163.

20 M. Zhang, C. Shao, J. Mu, Z. Zhang, Z. Guo, P. Zhang and Y. Liu, *Crystengcomm*, 2012, 14, 605-612.

21 J. Ma, L. Z. Zhang, Y. H. Wang, S. L. Lei, X. B. Luo, S. H. Chen, G. S. Zeng, J. P. Zou, S. L. Luo and C. T. Au, *Chem. Eng. J.*, 2014, 251, 371-380.

22 Z. Zhang, W. Wang, D. Jiang and J. Xu, *Catal. Commun.*, 2014, 55, 15-18.

23 D. Yue, D. Chen, Z. Wang, H. Ding, R. Zong and Y. Zhu, *Phys. Chem. Chem. Phys.*, 2014, 16, 26314-26321.

24 P. Zhang, C. Shao, M. Zhang, Z. Guo, J. Mu, Z. Zhang, X. Zhang and Y. Liu, *J. Hazard. Mater.*, 2012, 217, 422-428.

25 Y. S. Xu and W. D. Zhang, *Appl. Catal. B-Environ.*, 2013, 140, 306-316.

26 B. Yuan, C. Wang, Y. Qi, X. Song, K. Mu, P. Guo, L. Meng and H. Xi, *Colloid Surf. A-Physicochem. Eng. Asp.*, 2013, 425, 99-107.

27 H. G. Yu, Z. F. Zhu, J. H. Zhou, J. Wang, J. Q. Li and Y. L. Zhang, *Apl. Sur. Sci.*, 2013, 265, 424-430.

28 P. Wang, Y. Ao, C. Wang, J. Hou and J. Qian, *Carbon*, 2012, 50, 5256-5264.

29 M. Zhang, C. Shao, J. Mu, X. Huang, Z. Zhang, Z. Guo, P. Zhang and Y. Liu, *J. Mater. Chem.*, 2012, 22, 577-584.

30 G. Tian, Y. Chen, X. Meng, J. Zhou, W. Zhou, K. Pan, C. Tian, Z. Ren and H. Fu, *Chempluschem*, 2013, 78, 117-123.

31 Q. Yan, M. Sun, T. Yan, M. Li, L. Yan, D. Wei and B. Du, *Rsc Adv.*, 2015, 5, 17245-17252.

32 Y. Chen, G. Tian, Y. Shi, Y. Xiao and H. Fu, *Appl. Catal. B-Environ.*, 2015, 164, 40-47.

33 Z. Zhang, W. Wang, L. Wang and S. Sun, *ACS Appl. Mater. Interfaces*, 2012, 4, 593-597.

34 J. Cao, B. Xu, H. Lin, B. Luo and S. Chen, *Catal. Commun.*, 2012, 26, 204-208.

35 H. P. Jiao, X. Yu, Z. Q. Liu, P. Y. Kuang and Y. M. Zhang, *Rsc Adv.*, 2015, 5, 16239-16249.

36 J. Cao, B. Xu, H. Lin, B. Luo and S. Chen, *Dalton Trans.*, 2012, 41, 11482-11490.

37 H. Cheng, B. Huang, X. Qin, X. Zhang and Y. Dai, *Chem. Commmu.*, 2012, 48, 97-99.

38 B. G. Pejova, I. , *Mater. Chem. Phys.*, 2006, 99, 39-49.

39 X. Zong, H. Yan, G. Wu, G. Ma, F. Wen, L. Wang and C. Li, *J. Am. Chem. Soc.*, 2008, 130, 7176-7177.

40 H. Li, J. Liu, W. Hou, N. Du, R. Zhang and X. Tao, *Appl. Catal. B-Environ.*, 2014, 160, 89-97.

41 X. Wang, Q. Xu, M. Li, S. Shen, X. Wang, Y. Wang, Z. Feng, J. Shi, H. Han, and C. Li, *Angew. Chem. Int. Ed.*, 2012, 51, 13089-13092.

42 M. G. Ju, X. Wang W. Z. Liang, Y. Zhao and C. Li, *J. Mater. Chem. A*, 2014, 2, 17005-17014.

43 Y. Jia, S. Shen, D. Wang, X. Wang, J. Shi, F. Zhang, H. Han and C. Li, *J. Mater. Chem. A*, 2013, 1, 7905–7912.

44 X. Wang, S. Shen, S. Jin, J. Yang, M. Li, X. Wang, H. Han and C. Li, *Phys. Chem. Chem. Phys.*, 2013, 15, 19380-19386.

45 H. Zhao, L. Zhang, X. Gu, S. Li, B. Li, H. Wang, J. Yang and J. Liu, *RSC Adv.*, 2015, 5, 10951.

46 L. Zhang, K. H. Wong, Z. Chen, J. C. Yu, J. Zhao, C. Hu, C. Y. Chan and P. K. Wong, *Appl. Catal. A-Gen.*, 2009, 363, 221-229.

Graphical Abstract

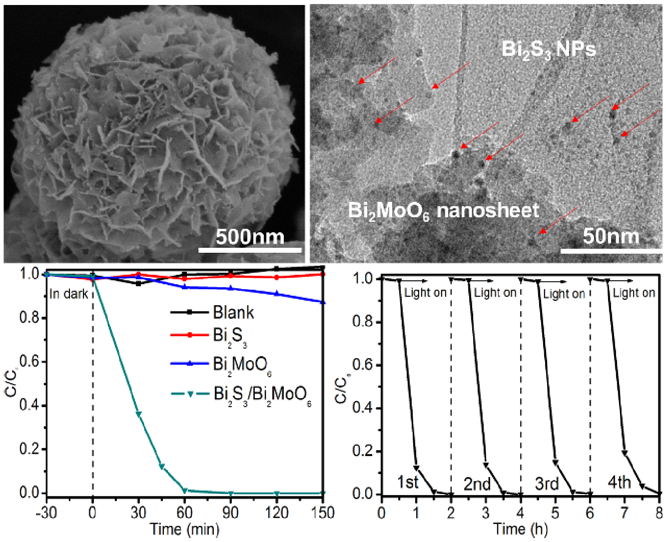

Flower-like Bi_2S_3/Bi_2MoO_6 heterojunction has been prepared via a solvothermal method and it exhibits stable and remarkable enhanced photocatalytic activity.